

# Chapter 11

## Nanowire-Based Lasers



Wenna Du, Jie Chen, Qing Zhang, and Xinfeng Liu

### 11.1 Introduction

In 1916, Albert Einstein predicted the existence of stimulated emission in theory, thus providing the underpinnings of lasing action [1]. By expanding the maser techniques to the infrared and optical region, Schawlow and Townes laid the solid foundation [2] for Theodore Maiman to demonstrate the first working laser successfully using a ruby gain material [3]. Till now, lasers have become ubiquitous in science and technology as well as in everyday life. They are vital for signal processing, communication, optical sensing, quantum optics, and metrology and are widely used for biological imaging, local surgery, metal welding, consumer electronics, and so on. From the time of its inception to the present day, there has been intense interest simultaneously in the miniaturization of the laser.

Thereafter, the success and widespread application of semiconductor lasers are mainly because they are much smaller and far cheaper and consume less power than any other kind of laser. One of the dominating areas of research among semiconductor lasers is the semiconductor nanowire laser: a quasi-one-dimensional semiconductor that simultaneously acts as an optical gain medium and optical cavity that, in some cases, possesses the intrinsic capability to lase [4–6]. These properties, along with the ability to tune the lasing wavelength and its possibility for electrical integration, make the semiconductor nanowire laser a promising candidate for use

---

W. Du · J. Chen · X. Liu (✉)

Division of Nanophotonics, CAS Key Laboratory of Standardization and Measurement for Nanotechnology, CAS Center for Excellence in Nanoscience, National Center for Nanoscience and Technology, Chinese Academy of Sciences, Beijing, China  
e-mail: [liuxf@nanoctr.cn](mailto:liuxf@nanoctr.cn)

Q. Zhang

Department of Materials Science and Engineering, College of Engineering, Peking University, Beijing, People's Republic of China

in the next generation of optoelectronic devices. They consist of submicron-sized “wires” typically formed from metal oxides, II–VI or III–V semiconductor alloys. Owing to the large difference in refractive index between the semiconductor and the embedding medium (usually free space or a low-refractive index dielectric material), the nanowire acts as both the optical gain medium and the optical cavity, thereby allowing lasing despite the limited volume of gain material. The first working of nanowire laser was observed [7] from ZnO nanowires grown from the “bottom up” on sapphire substrates coated with gold by simply heating a mixture of ZnO and graphite in an argon atmosphere [8]. The bottom-up growth method, which requires fewer post-processing steps than conventional diode lasers, can produce nearly defect-free, single-crystal heterostructures on virtually any kind of substrate, thus tremendously increasing the spatial design parameters. The natural anisotropy and the associated facets of the wurtzite structure of ZnO resulted in the formation of the nanowire optical cavity. Low-threshold operation is expected, owing to the small size of the active region of the semiconductor nanowire laser.

In this chapter, we introduce the concept of the nanowire laser and describe the basic mechanisms of lasing in semiconductor nanowires and most effective materials for nanowire lasers. Then, the wavelength controlling methods in semiconductor nanowire laser are discussed in detail. Improving the performance of the nanowire lasers furthermore, several new nanowire laser cavity structures, especially surface plasmon polariton lasers, are also described. Finally, we review some exciting new reports of electrically pumped nanowire lasers with the potential for integrated optoelectronic applications.

## 11.2 Nanowire Lasing Mechanisms

The three indispensable elements for nanowire lasers are pump source, gain medium, and optical cavity. The pump can be offered by a light source or a current source, the former of which is more often used for its easier realization while few researches has successfully realized nanowire lasers via electrically pumping. The other two indispensable elements can be satisfied by the nanowire itself due to nanowires’ inherent advantages such as big difference of refractive index with its environment, ultrasmooth surface, easily fabricated flat end facet, and high gain merits.

Usually, a single semiconductor nanowire with relatively high refractive index compared with environment is a natural FP cavity and consequently highlighted one key prerequisite for laser cavity design: the sub-wavelength optical confinement of the nanowire geometry. The main component is the FP cavity consisting of a gain medium between two opposite end faces. In the case of nanowires, the gain medium fills the entire cavity, and the opposite end-face reflections are from either parallel- or perpendicular-to-the-nanowire axis (see Fig. 11.1).

Besides, for a nanowire with radius close to or bigger than the semiconductor bandgap wavelength, a WGM cavity can be easily established within the cross-sectional plane of the nanowire. For example, Wiersig [10] reported WGM in

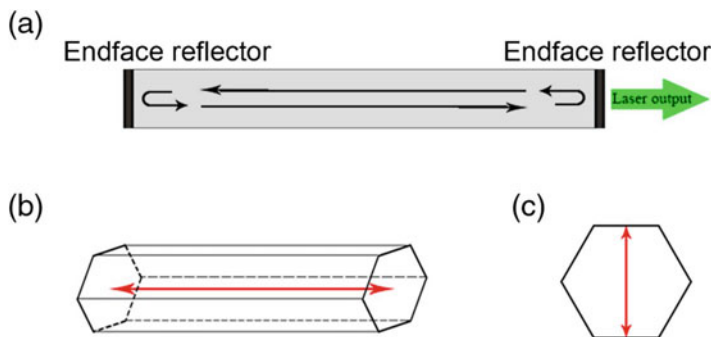


**Fig. 11.1** Semiconductor nanowire FP cavity. (a) Schematic of an FP cavity laser. (b) FP cavity formed by the nanowire's end faces. (c) FP cavity formed by the hexagon's end faces parallel to the wire axis. (Reprinted with permission from Ref. [9] Copyright 2006 by the American Chemical Society)

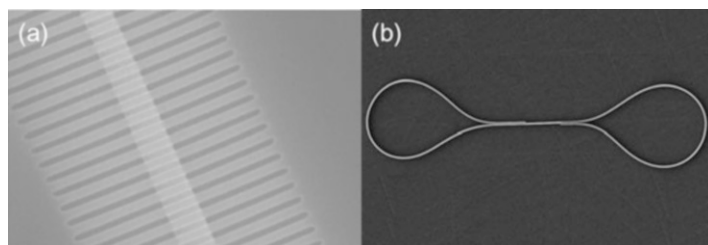


**Fig. 11.2** (a) Hybrid nanowire–photonic–crystal cavity. (Reprinted with permission from Ref. [11] Copyright 2006 by the American Chemical Society). (b) Nanowire loop mirror cavity. (Reprinted with permission from Ref. [12] Copyright 2011 by the American Chemical Society)

hexagonal dielectric cavities. Besides the abovementioned cavities, other geometries of optical cavities have also been fabricated, such as ring cavity, hybrid nanowire–photonic–crystal cavities, or nanowire loop mirror cavities (see Fig. 11.2).

### 11.2.1 Waveguiding Mechanism

By resolving Maxwell's equations using a similar formalism to an infinite circular waveguide, Ma and Maslov [5, 13] discussed the ability of the nanowire geometry to sustain multiple guided modes, depending on its diameter. Calculating the dispersion curves of the first guided modes ( $HE_{11}$ ,  $TE_{01}$ ,  $TM_{01}$ ) yields an estimate of the efficiency of light confinement in such sub-wavelength waveguides as shown in Fig. 11.3. Indeed, these dispersion curves reveal two interesting regimes. The first regime takes place below the cutoff diameter of the first transverse mode ( $TE_{01}$  mode), where only the fundamental  $HE_{11}$  mode is confined inside the nanowire,

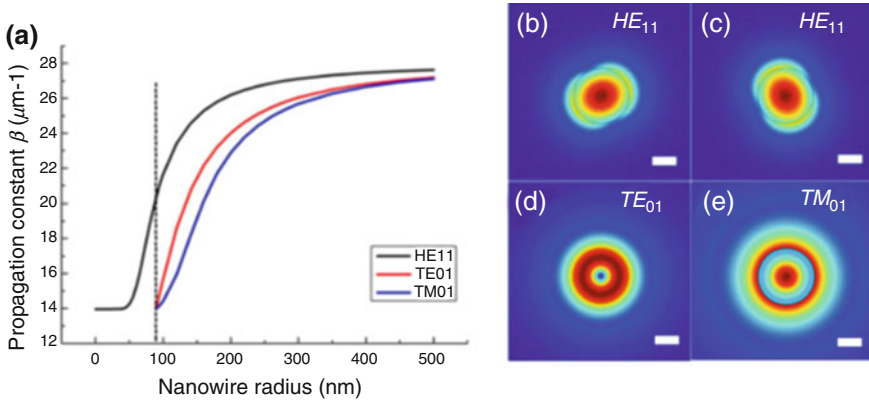


**Fig. 11.3** (a) Numerical solutions of propagation constant ( $\beta$ ) of the  $HE_{11}$ ,  $TE_{01}$ , and  $TE_{01}$  modes in an air-clad ZnO nanowire at 450 nm wavelength. Dashed line indicates the single-mode condition for the ZnO nanowire. (b)–(d) Electric field of the  $HE_{11}$ ,  $TE_{01}$ , and  $TE_{01}$  modes in an air-clad ZnO nanowire at 450 nm wavelength with 240 nm diameter. Scale bar, 100 nm. (Reprinted with permission from Ref. [5] Copyright 2013 by the Optical Society of America)

enabling the waveguide to have a single mode along the transverse axis. However, this mode's effective index is not maximized, meaning that the electric field extends considerably outside the nanowire and hence generates significant propagation loss. The second regime occurs above the cutoff frequency of the  $TE_{01}$  mode; at higher diameters, several guided modes are strongly confined inside the nanowire, with an effective index asymptotically approaching the semiconductor index, thus reducing the propagation losses of fundamental modes throughout the cavity. However, the presence of several guided modes increases the risk of the device operating in a multimode regime. Moreover, the various electric field distributions of confined modes that overlap with the gain medium will affect the device performance and favor mode competition via gain discrimination.

A simple method to achieve single-mode operation is the reduction of the resonator length, which can be realized by directly cutting the semiconductor nanowire. By this way, the free spectral range will increase to be larger enough to surpass the width of the gain profile and only one longitude mode left in the range finally. In 2012, Li realized a stable, single-mode output as shown in Fig. 11.4a–c, with  $\sim 0.12$  nm linewidth and  $> 18$  dB side-mode suppression ratio from a 135 nm wide, 4.7 mm long GaN nanowire, which is fabricated by a top-down technique [14]. Numerical simulations indicate that single-mode lasing arises from strong mode competition and narrow gain bandwidth. However, cutting the nanowire to several micrometers will lead to a relatively high threshold for the reduction of gain material and severe loss caused by end-face reflectivity effect [15]. For stable and single-mode lasers with lower lasing threshold and cavity losses, other methods are therefore preferable. One possible route in theory is to fabricate internal mode selection structure, e.g., distributed-Bragg-reflector (DBR) mirrors at the ends of

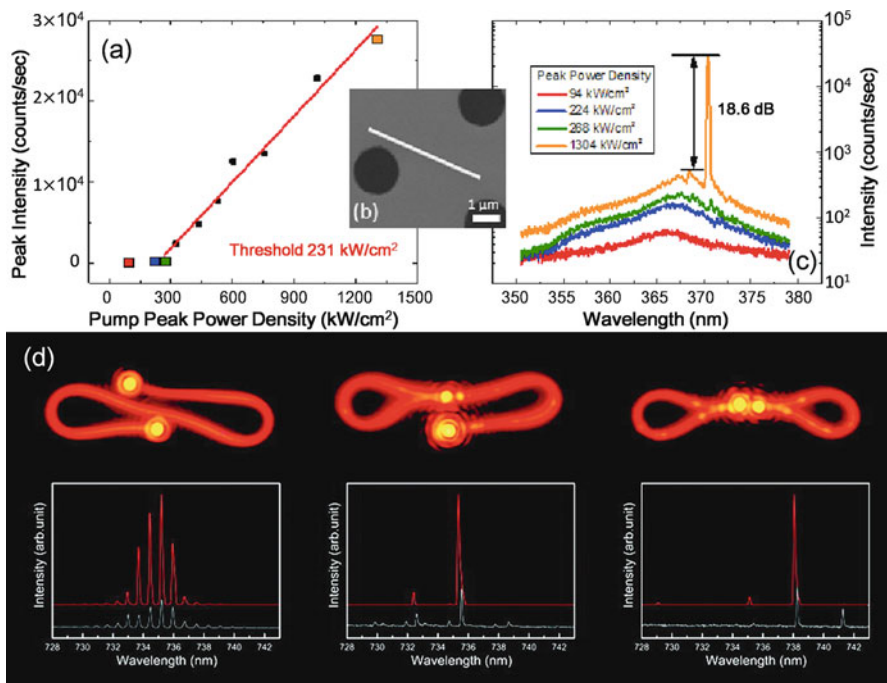


**Fig. 11.4** (a) Nanowire laser intensity versus pump laser intensity, for nanowires with lengths of 4.7  $\mu\text{m}$ . (b) Scanning electron micrographs of the GaN nanowire lasers. (c) Photoluminescence spectra from the nanowire lasers under uniform excitation for pump intensities as indicated in the figures. (Reprinted with permission from Ref. [14] Copyright 2012 by the Optical Society of America); (d) PL microscope images of lasing cavities and lasing spectra of single-nanowire structures without loop mirror, with one loop mirror, and with double loop mirrors. (Reprinted with permission from Ref. [12] Copyright 2011 by the American Chemical Society)

the nanowires for mode selection [16]. But it is very difficult to fabricate experimentally. Being inspired by the technique adopted on macroscopic lasing devices [17–19], in 2011, Xiao et al. [12] first induced the Vernier effect in the CdSe nanowire laser for fabrication of tunable single-mode nanowire lasers by folding the nanowire to form loop mirrors (see Fig. 11.4d). The Vernier effect will function when two or more cavities coupled together. The output modes must satisfy the oscillation conditions for all the cavities, and thus the number of modes will be greatly decreased. This effect is very attractive for the easiness to couple nanowire cavities and allowing sufficient gain.

It is noted that the waveguiding mechanism sets the nanowire diameter toward that of a single-nanowire laser. Despite the large refractive index difference between the nanowire's core and the surrounding medium (typically air), which favors strong confinement of the electric field, the diameter range for strong confinement of single or multiple guided modes has a minimum value and is scaled by the refractive index

and emission wavelength of the semiconductor. For instance, efficient waveguiding can be achieved for a 100-nm-diameter GaN nanowire emission and a minimum  $\sim$ 165-nm-diameter GaAs nanowire emission at 870 nm [20].

Another key figure of merit for nanowire lasers is the confinement factor  $\Gamma$  of the resonant modes, as a large  $\Gamma$  will favor a low threshold.  $\Gamma$  characterizes the overlap of the lasing mode with the gain medium, which for a nanowire depends strongly on its size and shape as well as on the electric field distribution of the resonant mode. For instance, a large confinement factor ( $\Gamma > 0.9$ ) could be achieved in a single-GaN nanowire cavity with a sufficiently large triangular cross section (cross-sectional size of 300 nm) for the TE<sub>01</sub> mode [21]. Robert et al. also presented that producing a large confinement factor is only meaningful when the polarization of the electromagnetic guided mode matches the polarization of the dipole transition of the semiconductor nanowire [22].

As we know, stimulated emission in semiconductors occurs when the Bernard–Durauffourg condition is achieved [23]. The optical susceptibility depends on the joint density of states as well as Fermi-level occupancy probabilities, in quasi-thermal equilibrium. This quasi-thermal equilibrium is necessary for obtaining stimulated emission via strong non-equilibrium carrier densities of electrons and holes. We recall that the density of states depends on the geometry of the structure, which is constant for 2D materials and inversely proportional to the square root of the energy in the case of one-dimensional (1D) nanowires [24]. This leads to Van Hove singularities, where resonant character of the absorption line makes the achievement of strong coupling possible even without formation of a bound state of an electron and a hole. If anything, this should support lasing in 1D nanowires where contrary to the case of conventional exciton polaritons, formation of 1D Van Hove polaritons can be realized in any system with a singularity in the density of states [25]. Under strong pumping condition, the exciton population can be very high, giving rise to the multiexciton interaction processes, such as stimulated emission, Auger recombination, and biexciton recombination. The processes decrease emission lifetime but compete with each other. As Fig. 11.5 shows, as pumping intensity is higher than  $28.0 \mu\text{J}/\text{cm}^2$ , exciton population inversion is reached, leading to amplified spontaneous emission and further lasing processes [26].

### 11.2.2 Gain and Losses

Amplification in a nanowire Fabry–Pérot cavity relies on the optical feedback from light reflected from the two crystalline end facets of the nanowire and propagated back through the gain medium. Lasing is achieved when the round-trip gain exceeds the round-trip losses [27]:

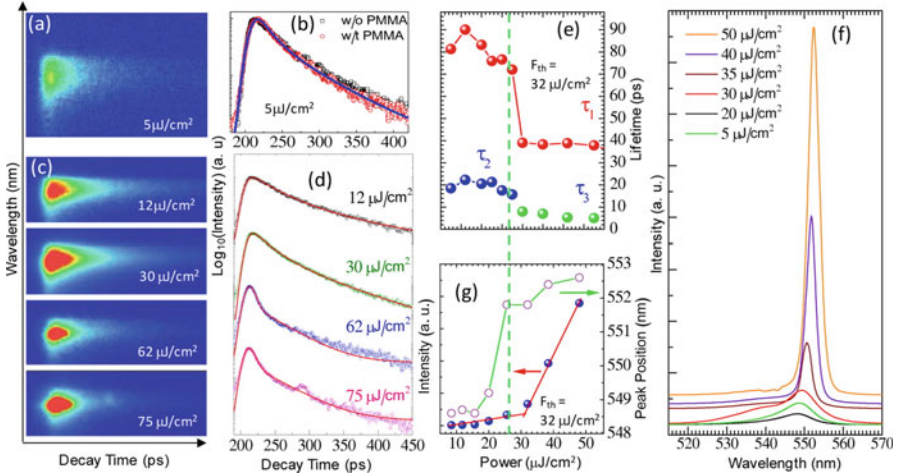


**Fig. 11.5** Power-dependent time-resolved PL spectroscopy of single ZnTe nanobelt. Streak camera image (a) and time-resolved PL spectra (b) of an individual ZnTe nanobelt. Power-dependent streak camera images (c) and the corresponding time-resolved PL spectra (d) of ZnTe nanobelt. (e) The PL lifetimes extracted as a function of power fluence. The green dashed line indicates the threshold of amplified spontaneous emission. (f) Power-dependent PL spectra of ZnTe nanobelt. (g) Intensity and peak position of PL emission as a function of pumping fluence extracted from (f) showing the amplified spontaneous emission. (Reprinted with permission from Ref. [26] Copyright 2012 by the American Chemical Society)

$$\Gamma g > \alpha_m + \alpha_p = \frac{1}{2L} \ln \left( \frac{1}{R_1 R_2} \right) + \alpha_p \tag{11.1}$$

where  $\Gamma$  is the confinement factor, i.e., the fraction of the mode intensity confined within the nanowire;  $g$  is the material gain;  $\alpha_m$  is the mirror loss;  $\alpha_p$  is the propagation loss by absorption or scattering, etc.;  $L$  is the cavity length; and  $R_1$  and  $R_2$  are the effective reflection coefficients for each end facet, which are nominally equal. As a result, increasing the gain efficiency or suppressing the round-trip loss may achieve lower threshold.

It has been suggested theoretically that the confinement factors for nanowire lasers are very large in comparison to those for heterostructure lasers and can even exceed unity [13]. The property of large confinement factors has been related to the strongly waveguiding nature of the nanowire, in which the actual length of wave propagation may exceed the axial length of the nanowire [28]. A larger-than-unity confinement factor suggests that modal gain (i.e., amplification specific to a given mode), in addition to material gain, may have a role in allowing a nanowire laser to reach the lasing threshold. In practice, this may aid nanowire lasers in achieving lasing, which would not be possible for different cavity geometry.

One way to increase gain efficiency is decreasing the temperature to dozens of kelvins to induce excitonic recombination [29, 30]. This kind of recombination, to

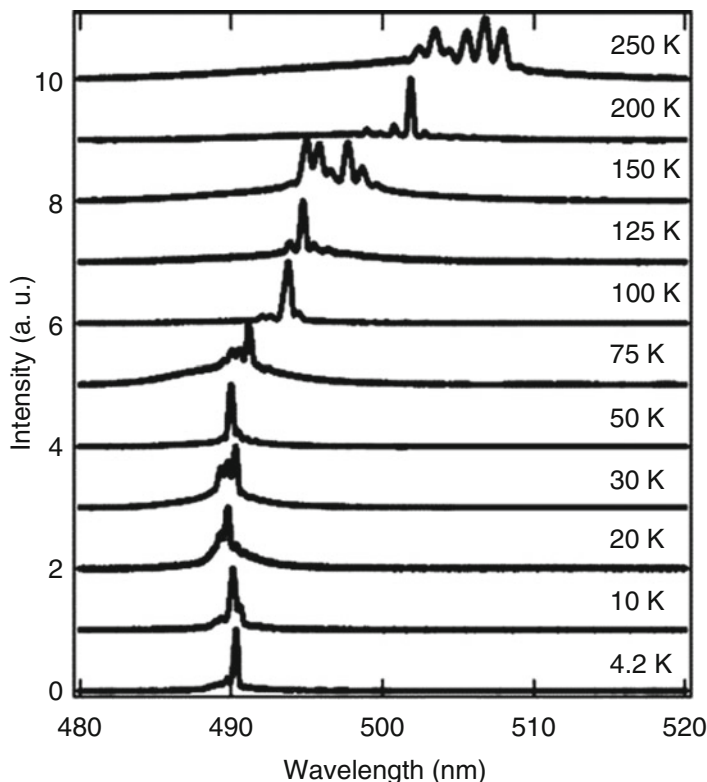


**Fig. 11.6** Temperature-dependent spectra recorded from a single CdS nanowire above the threshold for lasing. The temperature values are given next to each spectrum. The excitation power ranges from  $0.24 \mu\text{J}/\text{cm}^2$  at 4.2 K to  $3.3 \mu\text{J}/\text{cm}^2$  at 250 K. (Reprinted with permission from Ref. [26] Copyright 2005 by the American Chemical Society)

some extent, can avoid collision between electrons or holes with the lattice and thus more energy can be transferred to photons. In 2005, Agarwal investigated temperature-dependent PL/laser from the single cadmium sulfide (CdS) nanowire cavities [31]. As Fig. 11.6 shows, an exciton–exciton interaction was critical to lasing up to 75 K, while an exciton–phonon process dominates at higher temperatures. Below 75 K, a laser peak at 490.5 nm caused by exciton–exciton scattering was achieved, with a low threshold only at  $240 \text{ nJ}/\text{cm}^2$ .

To assess the losses due to photonic behaviors in the nanowire, we must consider the size of the whole nanowire cavity in the FP regime. First, the growth mechanism causes the nanowire to either lie on a substrate (horizontal geometry) or stand vertically for surface emission (vertical geometry). The interaction with the substrate in both cases induces severe optical losses, which considerably degrade the Q factor



and/or the absolute reflection coefficient at the nanowire–substrate interface. For vertical geometry, optical feedback can be reinforced for sufficiently large nanowire diameters with the appearance of high-order whispering gallerylike cavity modes, allowing stimulated emission for III–V (InGaAs) nanopillar on silicon [32]. A proposed alternative design is to insert a thin metallic layer between the substrate and the nanowire to increase the confinement factor  $\Gamma$ ; this part will be detailed later.

Given the gain efficiency and pump technique, suppressing optical loss  $\alpha$ , i.e., improving the cavity quality, can naturally decrease threshold for lasers. Compared with their bulk counterparts, the reflecting loss at semiconductor nanowires' end face is more severe because of strong end-face diffraction. Consequently, the Q factor, which is often used to evaluate the quality of cavity, is limited to below 1000 [27, 34–37]. To reach the laser threshold, the relatively low Q factor ( $< 100$ ) of the nanowire cavities requires the material gain to compensate for the cavity losses. Similarly, we must also mention that the inherent longitudinal multimode regime of the FP resonator, owing to the combination of cavity length and the rather broad linewidth of the nanowire emission profile at room temperature, is also detrimental to achieving efficient gain in nanowire lasers. One method to improve the Q factor is to manipulate the nanowire into ring geometry. Another method is to combine the nanowires with high-quality passive cavity, for example, embedding semiconductor nanowires into photonic crystal or hybridizing them with resonator. In 2006, Barrelet et al. combines chemically synthesized freestanding CdS nanowire emitter with lithographically defined 1D photonic crystal and racetrack micro-resonator structure [11] (see Fig. 11.7a, b). In his fabrication, localized emission and amplified spontaneous emission (ASE) at 4 K were successfully observed. Furthermore, Zhang in 2008 simulated a nano-cavity with ultrahigh Q factor via embedding a semiconductor nanowire in 1D photonic crystal [33] as shown in Fig. 11.7c–e. By defining 1D photonic crystal at the nanowire ends and engineering the microcavity pattern, the reflection on its end face could be improved by 20-folds, and a Q factor up to  $3 \times 10^5$  was designed.

As the study of single-nanowire lasers matures, it becomes increasingly important to rigorously model the nanowire laser. Modeling helps define the lasing threshold, which can be thought of as the amount of excitation necessary to turn the laser “on.” Specifically, modeling the transition from amplified spontaneous emission (ASE) to lasing oscillation enables a closer examination of the threshold behavior. When the spontaneous emission factor is large, as in the case of micro- and nanolasers, the definition of the lasing threshold becomes not consistent [39]. This lasing threshold is generally determined from a power plot describing the relationship between the input excitation and the output emission. For a nanoscale laser, the lasing threshold is less distinguished because the fraction of spontaneous emission coupled into a lasing mode becomes quite large. Rate equation analysis to model this relationship helps to define the lasing threshold of nanowire lasers. The coupled rate equations to describe the carrier density and photon density for a single mode in a semiconductor cavity can be defined as [38]

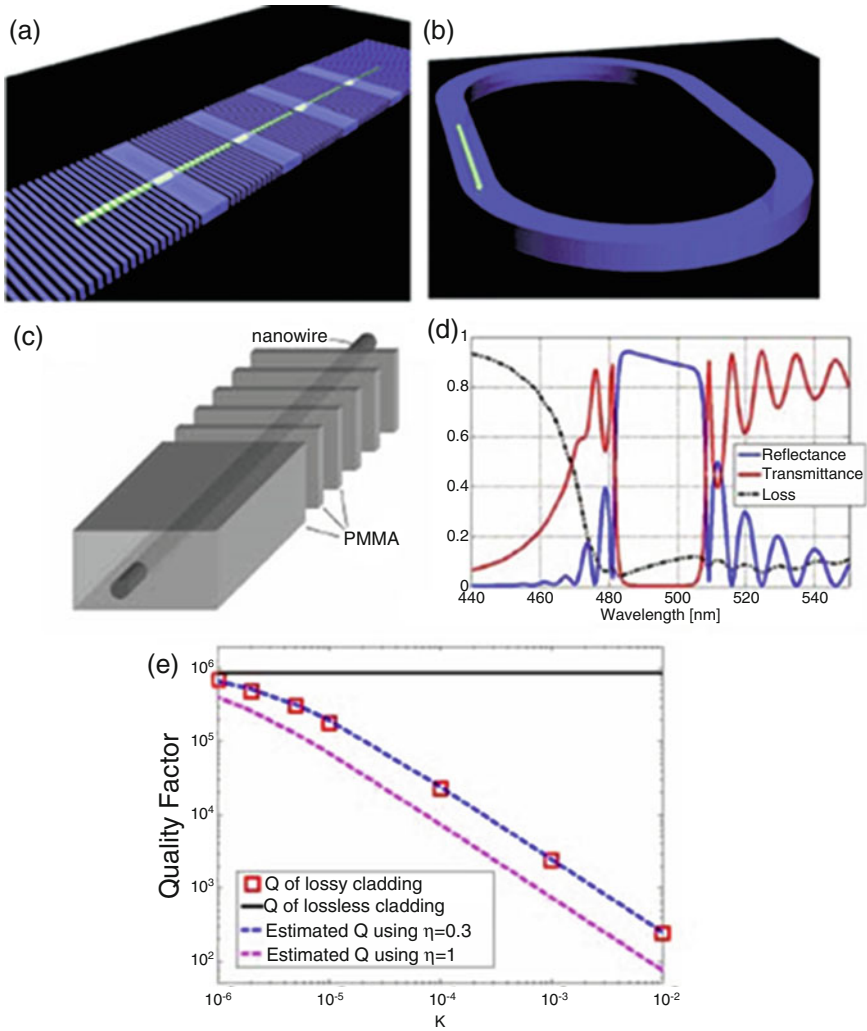
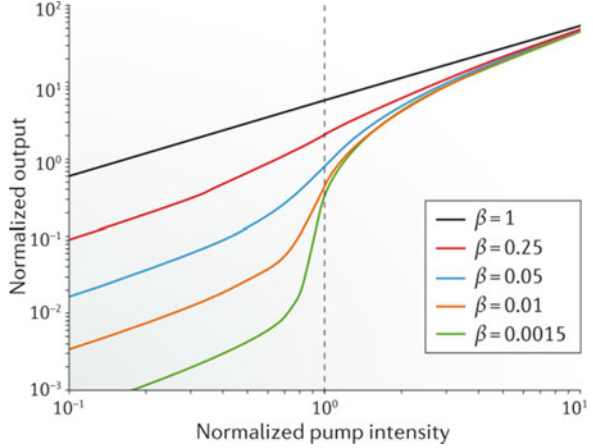


**Fig. 11.7** Nanowire photonic crystal (a) and micro-resonator (b) (Reprinted with permission from Ref. [11] Copyright 2006 by the American Chemical Society). (c) Schematic of a semiconductor nanowire with 1D photonic crystal defined at its end. (d) Transmittance and reflectance spectra for nanowire with photonic crystal consisting of 30 PMMA/air pairs. (e) Quality factor (red square) as a function of imaginary part of refractive index ( $\kappa$ ). The Q value with lossless cladding is indicated in black line. The dash lines represent estimation of Q using  $\eta = 0.3$  (blue) and 1 (magenta), respectively. (Reprinted with permission from Ref. [33] Copyright 2008 by the Optical Society of America) (Color figure online)

**Fig. 11.8** Calculated power plot of a hypothetical GaN laser with different values of  $\beta$ . (Reprinted with permission from Ref. [38] Copyright 2016 by the Macmillan Publishers Limited)



$$\frac{dN}{dt} = \eta P - \frac{N}{\tau_r} - \frac{N}{\tau_{nr}} - \Gamma v_g \alpha (N - N_0) S \tag{11.2}$$

$$\frac{dS}{dt} = \beta \frac{N}{\tau_r} + \Gamma v_g \alpha (N - N_0) S - \frac{1}{\tau_s} S \tag{11.3}$$

where  $N$  is the carrier density;  $S$  is the photon density;  $P$  is the pump intensity;  $\eta$  is the pumping efficiency;  $\tau_r$  and  $\tau_{nr}$  are the spontaneous emission and non-radiative lifetime, respectively;  $\tau_s$  is the photon lifetime;  $\beta$  is the spontaneous emission factor;  $N_0$  is the transparency carrier density;  $\alpha$  is the differential gain;  $\Gamma$  is the confinement factor; and  $v_g$  is the group velocity. The gain is approximated in the linear regime by Eq. 11.4:

$$g = \alpha(N - N_0) \tag{11.4}$$

By solving for these coupled rate equations under steady-state conditions, the photon density can be plotted as a function of pump intensity (see Fig. 11.8). The value of  $\beta$  is the fraction of spontaneous emission coupled into the laser mode of interest. A high  $\beta$ -value is crucial for applications, because it improves the nanowire laser emission efficiency and is also necessary for nanowire lasers with high modulation frequency [40]. By fitting the experimental power plot to a calculated plot, the lasing threshold can be more quantitatively defined. Quantum-optical (quantum-mechanical active medium and radiation field) theory of nanoscale lasers suggested that, even without a distinct threshold in the input versus output plot, it may be possible to determine a finite threshold.

To summarize, even though a nanowire laser appears to be an ideal nanosized laser, in practice, it is not as efficient as desired in current technology. Defects, surface states, multimode lasing, poor end-facet reflectivities, mode overlapping, and mode competition are many aspects that still must be addressed for improved device

efficiency. Much work remains to be done to unlock the full potential of semiconductor nanowire lasers.

### 11.3 Materials for Nanowire Lasers

Since the first demonstration of the bottom-up synthesis of semiconductor nanowires with high optical quality, it made possible to prepare new semiconductor materials suitable for nanowire lasers. This is particularly important for traditional semiconductors, such as ZnO and CdS. The use of relatively simple tube furnaces to grow nanowires of high crystalline quality is attractive for the initial exploration of new materials. The development of nanowire lasers made from GaN also represents the first extension of the single-nanowire laser to new material systems beyond ZnO [37]. One year later, the first example of lasing from a core-shell heterostructure that consisted of a GaN core with an epitaxial shell of  $\text{Al}_{0.75}\text{Ga}_{0.25}\text{N}$  was demonstrated [41]. Since these early studies, the library of nanowire laser materials has expanded enormously with emission wavelengths ranging from 370 to 2200 nm, resulting in nanolasers that emit in the ultraviolet (UV), visible, and near-infrared regions. This wide range in emission wavelengths can be seen in demonstrations for II–VI and III–V semiconductors and metal oxides, such as ZnO (REFS [7, 37, 42]), CdS (Ref. [11, 26, 31]), CdSe (Ref. [12, 43]), CdSSe (Ref. [44]), ZnS (Ref. [45]), GaN (REFS [14, 20, 21, 38, 46, 47]), InGaN (Ref. [48]), GaAs (Ref. [20, 49]), InGaAs (Ref. [32]), AlGaAs (Ref. [50]), GaSb (Ref. [51]), and InP (REFS [52, 53]). Stimulated emission due to two- and three-photon absorption with a high threshold of 100 mJ/cm<sup>2</sup> was reported in ZnO nanowires [42]. Zhang et al. further studied lasing performance of ZnO nanowires and demonstrated a lower threshold of 160  $\mu\text{J}/\text{cm}^2$  from two-photon absorption of ZnO nanowires pumped with a femtosecond pulse excitation at 700 nm [54]. Following these pioneering works, II–VI compounds became the focus of investigation, and Lieber's group at Harvard University first studied the lasing properties of CdS nanowires and the effect of temperature on the lasing threshold [55]. Stimulated emission in III–V compound nanowires was first reported in GaSb with lasing emission around telecommunication wavelengths (1570 nm) [51]. Chin et al. from the NASA Ames Research Center were the first to demonstrate low-temperature lasing emission of a III–V nanowire in the near-infrared range, with  $I_{\text{th}} = 50 \mu\text{J}/\text{cm}^2$  (see Fig. 11.9).

Recently, methyl ammonium lead halide perovskites were identified as a promising gain material for application in various optoelectronic systems [56–60]. These inorganic–organic hybrid materials exhibit high absorption cross sections, efficient photoluminescence, long diffusion lengths, and low trap-state densities [56]. Initial reports of ASE in hybrid perovskite thin films indicated that methyl ammonium lead iodide ( $\text{MAPbI}_3$ ) has high material gain with a low ASE threshold [58]. Recently, lasing in a perovskite nanowire cavity was reported for the first time, with the crucial breakthrough being the synthesis of nanowires with high optical quality and suitable dimensions [61]. Although they exhibit excellent

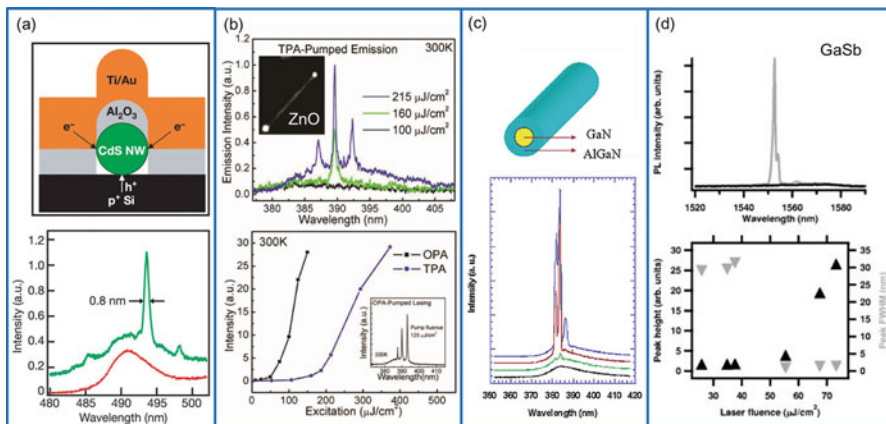


**Fig. 11.9** (a) Schematic showing the cross section of the device structure. Emission spectra from a CdS nanowire device with injection currents of 200  $\mu\text{A}$  (red) and 280  $\mu\text{A}$  (green) recorded at 8 K. (Reprinted with permission from Ref. [55] Copyright 2003 by the Macmillan Publishers Limited). (b) Two-photon pumped emission spectra for difference excitation fluence and integrated emission intensity from ZnO nanowires pumped by single-photon and two-photon processes versus excitation fluence. The inset shows the one-photon pumped lasing spectrum of ZnO nanowires. (Reprinted with permission from Ref. [54] Copyright 2009 by the Optical Society of America). (c) Schematic of the GaN/AlGaN core–sheath nanostructures, PL, and lasing spectra of individual nanowires excited by different power densities. (Reprinted with permission from Ref. [41] Copyright 2003 by the American Chemical Society). (d) GaSb nanowire NIR lasing and peak PL height at the lasing line wavelength of 1553 nm (black, up triangles) and PL width (gray, down triangles) vs laser fluence. (Reprinted with permission from Ref. [51] Copyright 2006 by the American Institute of Physics) (Color figure online)

performance, hybrid perovskite nanowires are well known for their intrinsic instability [62, 63]. Alternatively, the organic cation can be abandoned altogether, because cation replacement with cesium has opened up a new route to highly luminescent, stable materials [64]. The all-inorganic perovskite nanowires were found to be ultrastable under lasing conditions, continuing to lase even after  $10^9$  excitation cycles [65]. Mild growth conditions, excellent performance, and constantly increasing stability make perovskite-based nanowire lasers a promising material for the future.

### 11.4 Wavelength Tunability in Nanowire Lasers

For future nanolaser applications such as optical communication, environmental monitoring, and spectroscopy analysis, two key features must be considered: broadband emission and wavelength tunability. Different methods have been used to achieve tunability. Discrete color tunability can be achieved by using different gain materials, with the ultimate goal of achieving continuous wavelength tunability

to tailor emission to a specific application. Another approach to tune the wavelength is by modifying the dielectric environment of the cavity via the excitation intensity [37], cavity length [66], substrate properties [67], or cavity design [12, 68]. A simple route is changing the geometry of nanowire cavity depending on the FP cavity theory. As a kind of FP lasers, the wavelength of nanowire lasers must satisfy the stand-wave condition, that is,  $m\lambda = 2nL$ , where  $n$  is the refractive index,  $L$  is the length, and  $m$  is an integer. Therefore, wavelength tuning can be realized by modulating the optical length  $nL$ . Some physical mechanisms including absorption-emission-absorption process and Burstein–Moss effect have been utilized to tailor wavelength on a single nanowire with fixed composition. Li et al. achieved wide tuning of non-doped CdSe nanowire emission by shifting the pump spot position along the nanowire or by gradually cutting the NW shorter [66]. This tuned the lasing wavelength from 706 to 746 nm upon self-absorption of higher-energy photons by the nanowire and subsequent reemission of lower-energy photons, causing the emission wavelength to redshift. This method was also realized in CdS nanowires, where the lasing modes themselves could be similarly tailored [69]. They demonstrated an optical self-feedback mechanism based on the intrinsic self-absorption of the gain media to achieve low loss, room-temperature nanowire lasing with a mode selectivity over 30 nm. The CdS nanowire lasing wavelength was continuously tunable from 489 to 520 nm as the length of the nanowires increased from 4 to 25  $\mu\text{m}$ , as shown in Fig. 11.10. However, this strategy can only be applied for a limited wavelength range and can be impractical to implement in some cases.

Here, we focus our discussion on tuning the composition of the gain medium for controlling the emission wavelength. Synthesizing ternary or quaternary alloy nanowires with different stoichiometry ratios have been proved effectively to achieve nanowires with different bandgaps. The first is based on spatially graded alloy composition through careful control of the temperature gradient along the growth substrate. Compositional tunability in  $\text{CdS}_x\text{Se}_{1-x}$  nanowires on the same chip was demonstrated in 2005 [44]. These nanowire arrays exhibited chip position-dependent emission ranging from 498 to 692 nm depending on the composition (see Fig. 11.11a). In the same year, Liu et al. demonstrated a wavelength-controlled nanowire laser with  $\text{Zn}_x\text{Cd}_{1-x}\text{S}$  single-crystal nanoribbons [70]. The lasing emission of 485–515 nm and 340–390 nm was realized by combining laser ablation with thermal evaporation. These results suggest that  $\text{Zn}_x\text{Cd}_{1-x}\text{S}$  nanoribbon lasers of preselected “tunable” wavelengths between 340 and 515 nm may be achievable by tailoring the composition  $x$ . In addition, a composition gradient in the source material was also exploited to grow  $\text{In}_x\text{Ga}_{1-x}\text{N}$  alloy nanowires [71]. Multi-quantum-well core/shell nanowires were reported based on epitaxially growing highly uniform  $(\text{InGaN/GaN})_n$  outside triangular GaN nanowire cores [48]. PL spectra from nanowires with different In compositions have peak at different wavelengths. When the pump intensity reaches threshold, lasing operation occurs, and a redshift happens to the lasing wavelength with an increase in composition (Fig. 11.11c). The demonstrations of alloy composition control through a temperature gradient [44] and elemental gradient [70] enabled the growth of  $\text{Zn}_x\text{Cd}_x\text{S}_y\text{Se}_{1-y}$

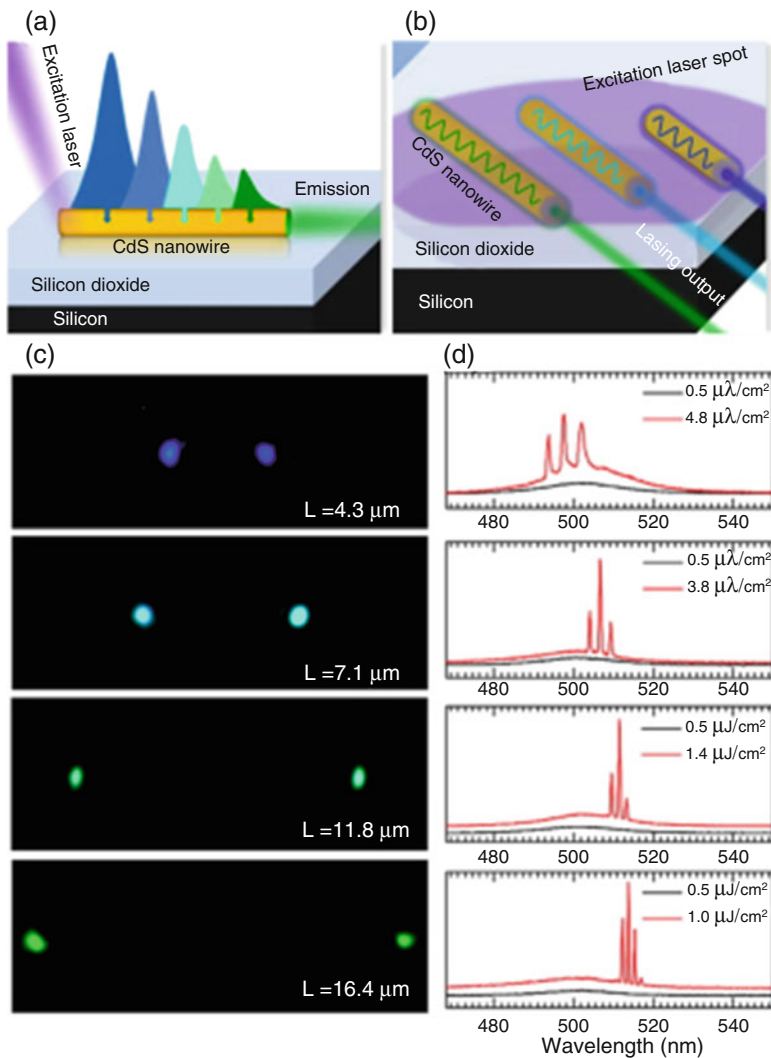


**Fig. 11.10** (a, b) Schematics the length-dependent lasing mode selections for CdS nanowires. When excited with laser pulses at one end (left end), the exciton–polaritons propagate inside the NWs and undergo scattering by the surface defects/phonons and subsequently self-absorption at the Urbach tail. Various output lasing colors are observed at the end facets of CdS NWs. (c, d) Optical images of four individual CdS NWs with different lengths undergoing lasing and the corresponding emission spectra. (Reprinted with permission from Ref. [69] Copyright 2013 by the American Chemical Society)

in its full composition range from ZnS to CdSe on a single substrate with emission spanning the full visible spectrum [72].

In addition, tuning the composition of the nanowires by changing the ratio of the halide salts in the growth sources enabled lasing across the visible and near-infrared

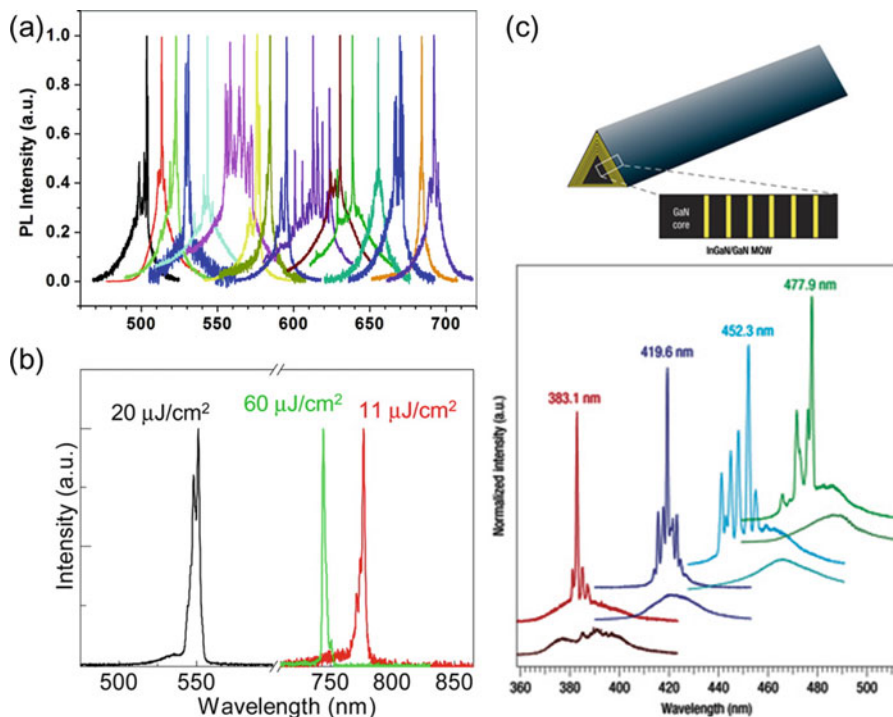


**Fig. 11.11** (a) CdS<sub>x</sub>Se<sub>1-x</sub> nanowires micro-PL collected at various locations along the substrate maintained at 77 K under high optical pumping condition showing lasing or multimode lasing. (Reprinted with permission from Ref. [44] Copyright 2009 by the American Chemical Society). (b) Lasing spectra of (CH<sub>3</sub>NH<sub>3</sub>PbI<sub>x</sub>Cl<sub>3-x</sub>) and (CH<sub>3</sub>NH<sub>3</sub>PbBr<sub>3</sub>). (Reprinted with permission from Ref. [58] Copyright 2015 by the American Chemical Society). (c) Schematic diagram of an InGaN/GaN MQW structure and normalized photoluminescence spectra collected from four representative 26MQW nanowire structures with increasing In composition pumped at different pumping powers. (Reprinted with permission from Ref. [48] Copyright 2008 by the Macmillan Publishers Limited)

spectrum [58, 61]. Xing and Liu et al. have realized room-temperature visible and near-infrared solid-state perovskite nanowire lasers. The lasing wavelength can be tuned from 777 to 744 nm (CH<sub>3</sub>NH<sub>3</sub>PbI<sub>x</sub>Cl<sub>3-x</sub>) and then 551 nm (CH<sub>3</sub>NH<sub>3</sub>PbBr<sub>3</sub>). Through precisely tuning the component ratio between Br and Cl (I) in CH<sub>3</sub>NH<sub>3</sub>PbBr<sub>x</sub>Cl<sub>3-x</sub> or CH<sub>3</sub>NH<sub>3</sub>PbI<sub>x</sub>Br<sub>3-x</sub>, fine-tuning of the lasing wavelength can be fulfilled (Fig. 11.11b).



## 11.5 New Nanowire Laser Cavity Structures

The physical manipulation of flexible nanowires provides a method for generating cavities of arbitrary geometry with improved performance. One example is the ring-resonator nanowire laser with higher Q factor. Ring resonators are typically formed by bending a pre-existing nanowire into a continuous loop. If the overlapping nanowire sections are sufficiently coupled to allow for recirculation of light around the loop, optical feedback is increased in the system, thereby lowering the lasing threshold. The first example of a nanowire ring resonator was made from GaN in 2006, which was manipulated into a loop with the two ends side by side [68]. Cavity modes were observed in the spontaneous emission and lasing spectra, indicating the formation of a circular resonator. The Q factor increased to 1300 approximately an order of magnitude larger than what is predicted for freestanding wires. Later, Ma et al. fabricated a pigtailed nanoribbon ring laser constructed with a 600 nm wide and 330 nm thick CdS nanoribbon [73] in 2010 (see Fig. 11.12). When the ring was pumped by a supercontinuum source, multi-longitudinal mode laser emission was observed around 523.5 nm with full widths at half maximum of 0.27 nm, corresponding to a Q factor of about 1900.

Alternative cavity geometries have also been explored to improve nanowire laser performance. Single-mode lasing is highly desirable for applications in sensing, optical communications, spectroscopy, and interferometry. One alternative strategy relies on the formation of a cleaved-coupled cavity [46]. By cleaving a nanowire at a determined point, all but a single lasing mode may be suppressed by modulating the loss at the air gap. Successful device fabrication relies on calculations of both the gap position and the size of each cavity to modulate the lasing threshold of all the longitudinal modes. This process was recently shown for a GaN nanowire that was cleaved using focused ion-beam milling. Another strategy to achieve single-mode lasing relies on the use of “loop mirrors,” in which the nanowire is bent into a loop, resulting in both high effective reflectivity and a shortened cavity path length [12]. By bending a CdSe nanowire to include zero, one or two loop mirrors, a threefold decrease in the lasing threshold and near single-mode lasing were observed. Emission occurred at 738 nm with a linewidth of only 0.12 nm and a threshold of 34.4  $\mu\text{J}/\text{cm}^2$ .

In 2008, Yang Q et al. coupled several ZnO nanowires with a silica microfiber knot cavity just by attaching them together through the Van der Waals force [74]. This hybrid structure combines advantages of high gain of nanowires and high-quality factor of microfiber knot cavities. By pumping the nanowires with a 355 nm wavelength laser pulses, Q factor up to  $10^4$  and a threshold lower than 0.2 mJ/pulse were successfully achieved. This design offers convenient and efficient approach to both pumping and collection of the nanowire lasers and has shown big potential for optical integration in the future. By substituting the microfiber knot to a high-Q silica microdisk cavity, the threshold can be further decreased [75].

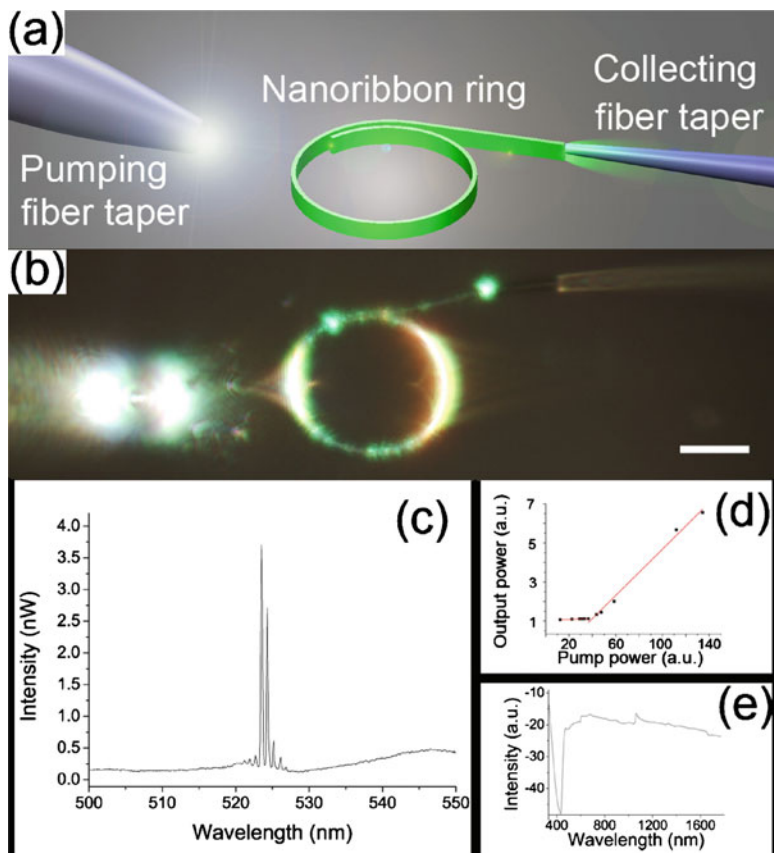


**Fig. 11.12** Pigtailed CdS nanoribbon ring laser. (a) Schematic of the structure of the nanoribbon ring laser system. (b) Optical micrographs of a 20  $\mu\text{m}$  diameter CdS nanoribbon ring under pumping; scale bar, 10  $\mu\text{m}$ . (c) Collected lasing spectra of the nanoribbon ring. (d) Integrated emission power versus pump energy of the nanoribbon ring laser. (e) Spectrum of the pumping light from the supercontinuum source. (Reprinted with permission from Ref. [73] Copyright 2010 by the AIP Publishing LLC)

Meantime, by combining the bandgap engineering and cavity parameters, Liu et al. [76] demonstrated lasing emission between red and green colors separated by 107 nm in wavelength simultaneously in a single bandgap-graded  $\text{CdS}_x\text{Se}_{1-x}$  nanowire (see Fig. 11.13). By looping the wide-gap end of the alloy nanowire through nanoscale manipulation, two relatively isolated cavities were formed, providing lasing oscillations at two different wavelengths. The total output color can be continuously tuned by changing the relative pumping powers of the two cavities.

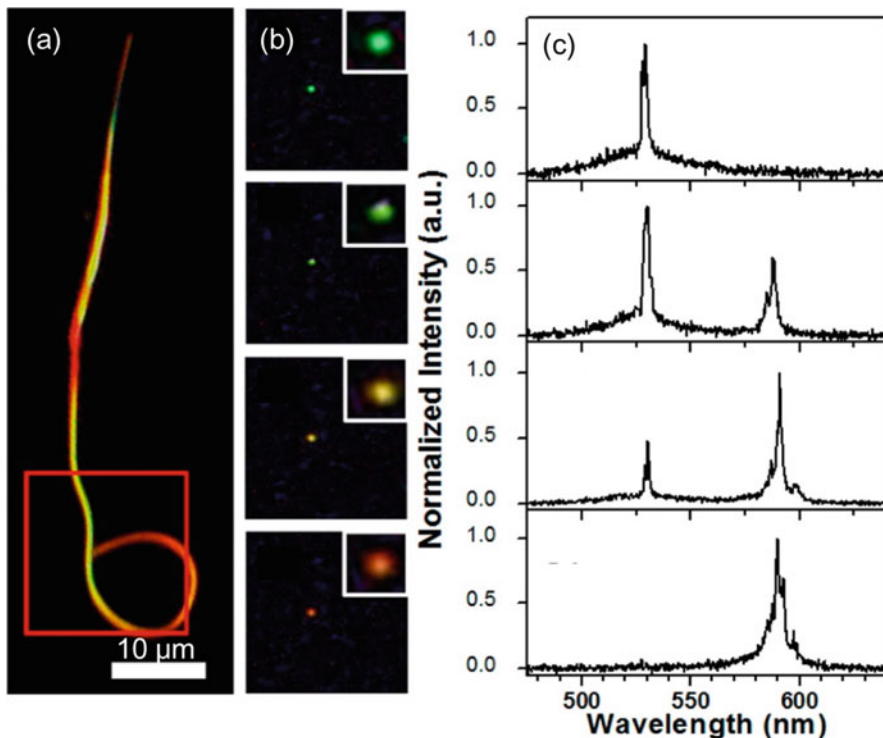


**Fig. 11.13** Color control of a looped  $\text{CdS}_x\text{Se}_{1-x}$  wire dual-color laser. (a) Dark-field image of the looped nanowire. (b) Real-color images of the lasing under different pumping for the two cavities taken from the red box in (a). (c) Normalized lasing spectra under different controlled pumping intensities. (Reprinted with permission from Ref. [76] Copyright 2013 by the American Chemical Society) (Color figure online)

## 11.6 Surface Plasmon Polariton Lasers

The miniaturization of semiconductor nanowire lasers is limited by the diffraction limit, which is approximately half of the optical wavelength in the medium. In general, reducing the diameter of the nanowire leads to poor optical confinement and small modal gain, which make photonic lasing impossible. However, nanowires can be used as platforms for creating a new type of laser based on surface plasmon polaritons (SPPs) [77, 78]. SPP waves, which are the collective oscillations of conduction electrons on the surface of a metal, lead to enhanced electromagnetic fields confined at sub-wavelength nanoscale, which allows the laser cavity to store and guide optical energy far below the optical diffraction limit. The strategy of applying a silver coating to a nanowire laser to harness SPPs for lasing and to reduce the overall size of the laser structure was first studied theoretically [79] in 2007. This study suggested the existence of wavelength regions in which the nanowire optical

gain could exceed the metal loss—the process of optical energy absorption and dissipation via electron scattering and thermalization in a metal—to achieve an overall positive gain.

Early theoretical work predicted that a dielectric–metal hybrid structure could be a successful platform for lasing [80]. This was followed by the first report of SPP nanowire lasing in a horizontal CdS nanowire on a silver substrate, separated by a nanoscale film of  $\text{MgF}_2$  that provides control over optical confinement, insulates the wire from the metal, and provides a transverse hybrid cavity [81]. Through optical pumping, characteristic signatures of lasing were observed that indicated that the plasmonic nanowires were operating in Fabry–Pérot geometry.

Meantime, combining semiconductor nanowire with metal structures to generate SPP can be a possible route to increase the confinement factor  $\Gamma$  by leading to larger overlap between the mode and the gain material. SPP may also increase the lasers' tolerance to low cavity quality. Noticeably, for the practical realization of low-threshold lasing operation based on SPP, ohmic loss accompanying with it should be effectively suppressed. In 2008, a creative approach hybridizing dielectric waveguiding with plasmonics has been proposed [80]. In 2012, Yu et al. demonstrated a semiconductor nanowire laser with ultralow threshold which can be reached by CW pump at low temperature [82]. The semiconductor nanowire used in his design is a GaN nanorod partially filled with InGaN as gain medium and separated by a 5 nm silicon dioxide ( $\text{SiO}_2$ ) spacer from an atomically smooth epitaxial silver film to avoid unnecessary SPP scattering. The SPPs excited in noble metal structure adjacent to gain media have dramatically reduced the optical mode volume and thus improve the overlap between mode and gain medium. Laser action has been achieved even under CW pump (405 nm). By locating triangular GaN nanowire on Al film with a spacer layer of  $\text{SiO}_2$ , Zhang et al. [83] demonstrated the first strong room-temperature UV ( $\sim 370$  nm) plasmonic laser with an extremely low threshold ( $\sim 3.5 \text{ MW/cm}^{-2}$ ). In the plasmonic devices, the ohmic losses and scattering/radiation losses are efficiently suppressed through reducing the surface roughness of the metal and  $\text{SiO}_2$ ; meanwhile, the gain compensation is greatly enhanced because of the flat metal–insulator–semiconductor interface.

Furthermore, SPs have proved their capability to manipulate the nanowire cavity mode and further the lasing wavelength. As shown in Fig. 11.14a, Zhang et al. demonstrated that an Ag NP in the vicinity of a CdS nanowire can simultaneously modulate the effective cavity length, equivalent phase shift, and the Q factor of the cavity modes [84]. Ag NP acts as a reflective and half-reflective nanomirror when it is located at the end and at the side of the CdS nanowire cavity, respectively. When the CdS nanowire is sitting on Au film with insulator  $\text{SiO}_2$  thin layer as spacer, the Burstein–Moss effect inside the CdS nanowires can be enhanced by the extremely confined electric field in the nanometer-thick insulator layer. The hybrid semiconductor–insulator–metal structures are well-known to support the low-loss SPP. The enhanced Burstein–Moss effect leads to a larger blueshift of the output photonic lasing wavelength of the CdS nanowires. The enhancement factor increases with the decrease of the  $\text{SiO}_2$  thickness as a result of the increase of localized electric field and exciton–plasmon interaction strength. Through varying the thickness of

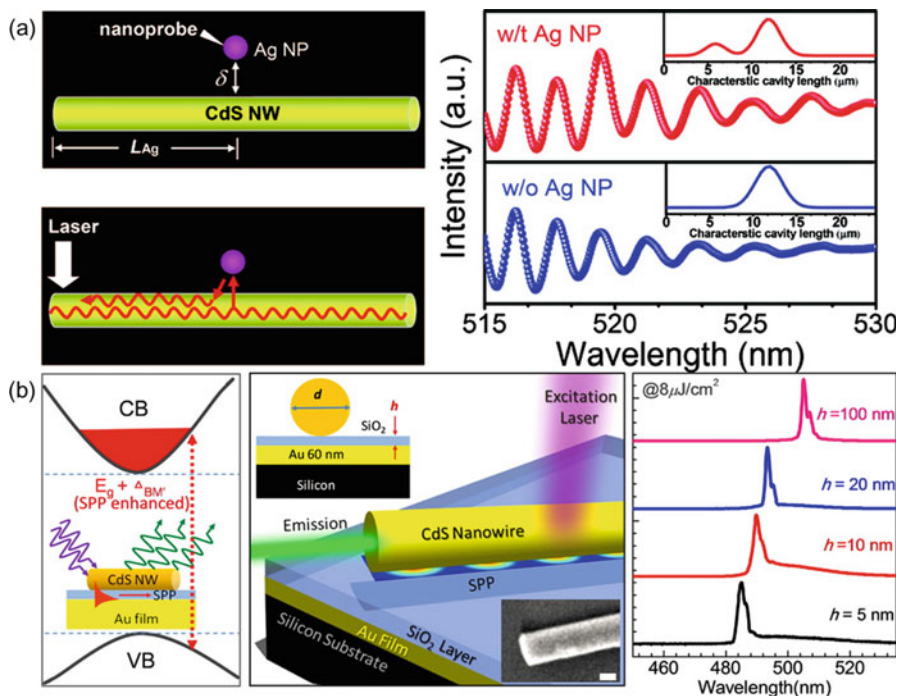


**Fig. 11.14** Localized surface plasmon and surface plasmon polariton-modulated cavity modes of CdS nanowire cavity. (a) Schematic illustration of the CdS NW–Ag NP hybrid microcavity fabricated with a nanoprobe and modulations of PL Fabry–Pérot oscillation in the CdS NW by an Ag NP located nearby the side surface of the NW and normalized PL spectra at the right end of the NW in the presence or absence of Ag NP when a focused 488 nm laser is illuminated at the middle part of the NW. (Reprinted with permission from Ref. [84] Copyright 2011 by the American Chemical Society). (b) The enhanced Burstein–Moss effect and the observation of strong Purcell effect with the presence of the localized electric. The lasing peaks of four devices are blueshift as a consequence. (Reprinted with permission from Ref. [67] Copyright 2013 by the American Chemical Society)

SiO<sub>2</sub> from 100 to 5 nm, the lasing wavelength was tuned from 504 to 483 nm. Tunability of ~30 nm was obtained [67] (see Fig. 11.14b).

## 11.7 Electrical Excitation of Nanowire Lasers

The nanowire lasers discussed thus far are excited optically by another laser that is orders of magnitude larger. Optical excitation is unsuitable for most of the intended nanowire laser applications, especially in the area of on-chip integrated photonics. The ultimate goal for semiconductor nanowire lasing hinges on achieving reliable lasing through the electrical injection of electrons and holes into a dielectric–metal

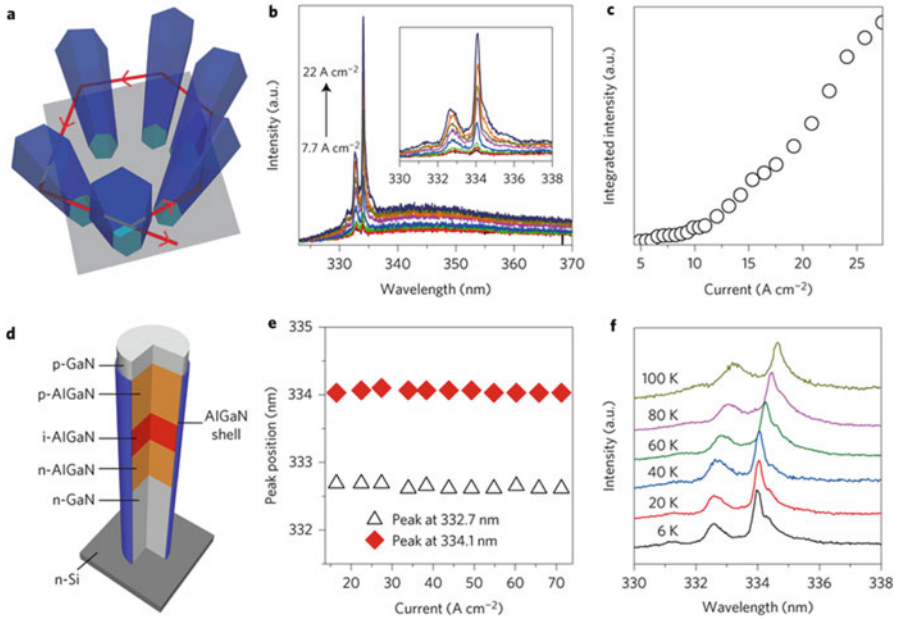


**Fig. 11.15** (a, d) Schematic diagram illustrating the formation of a closed-loop path inside AlGaIn nanowire arrays and AlGaIn nanowire double heterostructures. (b) Emission spectra measured at 6 K under different current densities. (c) Integrated intensity of the lasing peak at 334.1 nm as a function of injection current density. (e) Plot of peak position versus current density. (f) EL spectra measured at different operation temperatures. (Reprinted with permission from Ref. [87] Copyright 2015 by the Nature Publishing Group)

composite nanowire structure. Similar to plasmonic lasers, metal loss has been identified as the primary loss mechanism in electrically pumped cavities [85]. Overcoming this has been a high priority and has been pursued through several different approaches.

Lithographic, top-down techniques are currently the most viable approach for producing electrically driven nanowire lasers. In the first report of electrically pumped nanowire lasing around 509 nm, a horizontal CdS nanowire on a Si ( $p^{2+}$ ) substrate was coated with an insulating layer of  $Al_2O_3$  followed by a Ti–Au injection layer [55]. Almost a decade passed before promising device architecture arose, the semiconductor core–metal shell [79] structure, which was realized using a top-down fabrication process [86].

Another strategy for electrical pumping relies on nanowire arrays grown directly on conducting substrates followed by post-synthetic introduction of the second contact. Highly stable, electrically pumped random lasing in AlGaIn nanowire arrays has recently been reported [87]. As shown in Fig. 11.15, by using the Anderson localization of light in AlGaIn–GaN heterostructures, random lasing in the UV spectral region was achieved in a lithography-free nanowire array. Successful continuous-wave operation was observed from 6 to 100 K, with a lasing threshold

of  $12 \text{ A cm}^{-2}$  and an operational stability at over six times the threshold current. Emission wavelength tunability across the entire ultraviolet AII (UV-AII) band ( $\sim 320\text{--}340 \text{ nm}$ ) was also observed for various regions depending on the nature of the gain cavity.

## References

1. Einstein A (1916) Strahlungs-Emission und -Absorption nach der Quantentheorie, vol 18
2. Schawlow AL, Townes CH (1958) Infrared and optical masers
3. Maiman TH (1960) Stimulated optical radiation in ruby. *Nature* 187(4736):493–494
4. Ning CZ (2012) Semiconductor nanowire lasers. *Semicond Semimetals* 86:455–486
5. Tong L, Dai L, Wu X, Guo X, Ma Y (2013) Semiconductor nanowire lasers. *Adv Opt Photon* 3(3):216–273
6. Yan R, Gargas D, Yang P (2009) Nanowire photonics. *Nat Photonics* 3(3):569–576
7. Huang MH, Mao S, Feick H, Yan H, Wu Y, Kind H, Weber E, Russo R, Yang P (2001) Room-temperature ultraviolet nanowire nanolasers. *Science* 292(5523):1897
8. Huang MH, Wu Y, Feick H, Tran N, Weber E, Yang P (2001) Catalytic growth of zinc oxide nanowires by vapor transport. *Adv Mater* 13(2):113–116
9. van Vugt LK, Rühle S, Vanmaekelbergh D (2006) Phase-correlated nondirectional laser emission from the end facets of a ZnO nanowire. *Nano Lett* 6(12):2707–2711
10. Wiersig J (2002) Hexagonal dielectric resonators and microcrystal lasers. *Phys Rev A* 67(2):426–430
11. Barrelet CJ, Bao JM, Loncar M, Park HG, Capasso F, Lieber CM (2006) Hybrid single-nanowire photonic crystal and microresonator structures. *Nano Lett* 6(1):11–15. <https://doi.org/10.1021/nl0522983>
12. Xiao Y, Meng C, Wang P, Ye Y, Yu H, Wang S, Gu F, Dai L, Tong L (2011) Single-nanowire single-mode laser. *Nano Lett* 11(3):1122
13. Maslov AV, Ning CZ (2004) Modal gain in a semiconductor nanowire laser with anisotropic band structure. *IEEE J Quantum Electron* 40(10):1389–1397
14. Li Q, Wright JB, Chow WW, Luk TS, Brener I, Lester LF, Wang GT (2012) Single-mode GaN nanowire lasers. *Opt Express* 20(16):17873
15. Wang S, Hu Z, Yu H, Fang W, Qiu M, Tong L (2009) Endface reflectivities of optical nanowires. *Opt Express* 17(13):10881–10886
16. Chen L, Towe E (2006) Nanowire lasers with distributed-Bragg-reflector mirrors. *Appl Phys Lett* 89(5):89
17. Wu X, Li H, Liu L, Xu L (2008) Unidirectional single-frequency lasing from a ring-spiral coupled microcavity laser. *Appl Phys Lett* 93(8):1710
18. Wu X, Sun Y, Suter JD, Fan X (2009) Single mode coupled optofluidic ring resonator dye lasers. *Appl Phys Lett* 94(24):381
19. Huang D, Xu E, Zhou L, Li X, Zhang X, Zhang Y, Yu Y (2010) Ultrahigh-Q microwave photonic filter with Vernier effect and wavelength conversion in a cascaded pair of active loops. *Opt Lett* 35(8):1242–1244
20. Lang RJ, Yariv A (2002) An exact formulation of coupled-mode theory for coupled-cavity lasers. *IEEE J Quantum Electron* 24(1):66–72
21. Seo MK, Yang JK, Jeong KY, Park HG, Qian F, Ee HS, No YS, Lee YH (2008) Modal characteristics in a single-nanowire cavity with a triangular cross section. *Nano Lett* 8(12):4534
22. Röder R, Ploss D, Kriesch A, Buschlinger R, Geburt S, Peschel U, Ronning C (2014) Polarization features of optically pumped CdS nanowire lasers. *J Phys D Appl Phys* 47(39):394012

23. Bernard MGA, Duraffourg G (2010) 10–laser conditions in semiconductors \*. *Essentials of Lasers* 1(7):699–703
24. Couteau C, Larrue A, Wilhelm C, Soci C (2015) Nanowire lasers. *Nano* 4(1):90–107
25. Arnardottir KB, Kyriienko O, Portnoi ME, Shelykh IA (2013) One-dimensional Van Hove polaritons. *Phys Rev B* 87(12):125408
26. Zhang Q, Liu X, Utama MI, Zhang J, De IMM, Arbiol J, Lu Y, Sum TC, Xiong Q (2012) Highly enhanced exciton recombination rate by strong electron-phonon coupling in single ZnTe nanobelt. *Nano Lett* 12(12):6420
27. Maslov AV, Ning CZ (2003) Reflection of guided modes in a semiconductor nanowire laser. *Appl Phys Lett* 83(6):1237–1239
28. Ning CZ, Ding K, Fan F, Liu ZC (2014) Semiconductor Nanolasers (a tutorial), *Photonics Society Summer Topical Meeting Series*, pp 23–24
29. Kayanuma Y (1988) Quantum-size effects of interacting electrons and holes in semiconductor microcrystals with spherical shape. *Phys Rev B Condens Matter* 38(14):9797
30. Wegscheider W, Pfeiffer LN, Dignam MM, Pinczuk A, West KW, McCall SL, Hull R (1993) Lasing from excitons in quantum wires. *Phys Rev Lett* 71(24):4071
31. Agarwal R, Barrelet CJ, Lieber CM (2005) Lasing in single cadmium sulfide nanowire optical cavities. *Nano Lett* 5(5):917
32. Changhasnain CJ (2011) Nanolasers grown on silicon. *Nat Photonics* 5(3):170–175
33. Lončar M, Zhang Y (2008) Ultra-high quality factor optical resonators based on semiconductor nanowires. *Opt Express* 16(22):17400
34. Wang MQ, Huang YZ, Chen Q, Cai ZP (2006) Analysis of mode quality factors and mode reflectivities for nanowire cavity by FDTD technique. *IEEE J Quantum Electron* 42(2):146–151
35. Li ZY, Ho KM (2005) Bloch mode reflection and lasing threshold in semiconductor nanowire laser arrays. *Phys Rev B* 71(4)
36. Ding Y, Motohisa J, Hua B, Shinjiroh Hara A, Fukui T (2007) Observation of microcavity modes and waveguides in InP nanowires fabricated by selective-area metalorganic vapor-phase epitaxy. *Nano Lett* 7(12):3598–3602
37. Johnson JC, Yan HQ, Yang PD, Saykally RJ (2003) Optical cavity effects in ZnO nanowire lasers and waveguides. *J Phys Chem B* 107(34):8816–8828. <https://doi.org/10.1021/jp034482n>
38. Eaton SW, Fu A, Wong AB, Ning CZ, Yang PD (2016) Semiconductor nanowire lasers. *Nat Rev Mater* 1(6):Art16028. <https://doi.org/10.1038/Natrevmats.2016.28>
39. Ning CZ (2013) What is laser threshold? *Ieee J Sel Top Quant* 19(4):Art1503604. <https://doi.org/10.1109/Jstqe.2013.2259222>
40. Chow WW, Jahnke F, Gies C (2014) Emission properties of nanolasers during the transition to lasing. *Light-Sci Appl* 3:ARTN e201. <https://doi.org/10.1038/lsa.2014.82>
41. Choi HJ, Johnson JC, He RR, Lee SK, Kim F, Pauzauskie P, Goldberger J, Saykally RJ, Yang PD (2003) Self-organized GaN quantum wire UV lasers. *J Phys Chem B* 107(34):8721–8725. <https://doi.org/10.1021/jp034734k>
42. Zhang CF, Dong ZW, You GJ, Qian SX, Deng H (2006) Multiphoton route to ZnO nanowire lasers. *Opt Lett* 31(22):3345–3347. <https://doi.org/10.1364/Ol.31.003345>
43. Pan AL, Liu RB, Zhang QL, Wan Q, He PB, Zacharias M, Zou BS (2007) Fabrication and red-color lasing of individual highly uniform single-crystal CdSe nanobelts. *J Phys Chem C* 111(38):14253–14256. <https://doi.org/10.1021/jp0740548>
44. Pan AL, Zhou WC, Leong ESP, Liu RB, Chin AH, Zou BS, Ning CZ (2009) Continuous alloy-composition spatial grading and Superbroad wavelength-tunable nanowire lasers on a single Chip. *Nano Lett* 9(2):784–788. <https://doi.org/10.1021/nl803456k>
45. Zapien JA, Jiang Y, Meng XM, Chen W, Au FCK, Lifshitz Y, Lee ST (2004) Room-temperature single nanoribbon lasers. *Appl Phys Lett* 84(7):1189–1191. <https://doi.org/10.1063/1.1647270>
46. Gao HW, Fu A, Andrews SC, Yang PD (2013) Cleaved-coupled nanowire lasers. *P Natl Acad Sci USA* 110(3):865–869. <https://doi.org/10.1073/pnas.1217335110>



47. Gradecak S, Qian F, Li Y, Park HG, Lieber CM (2005) GaN nanowire lasers with low lasing thresholds. *Appl Phys Lett* 87(17):Artn 173111. <https://doi.org/10.1063/1.2115087>
48. Qian F, Li Y, Gradecak S, Park HG, Dong YJ, Ding Y, Wang ZL, Lieber CM (2008) Multi-quantum-well nanowire heterostructures for wavelength-controlled lasers. *Nat Mater* 7(9):701–706. <https://doi.org/10.1038/nmat2253>
49. Saxena D, Mokkalapati S, Parkinson P, Jiang N, Gao Q, Tan HH, Jagadish C (2013) Optically pumped room-temperature GaAs nanowire lasers. *Nat Photonics* 7(12):963–968. <https://doi.org/10.1038/Nphoton.2013.303>
50. Mayer B, Rudolph D, Schnell J, Morkotter S, Winnerl J, Treu J, Muller K, Bracher G, Abstreiter G, Koblmuller G, Finley JJ (2013) Lasing from individual GaAs-AlGaAs core-shell nanowires up to room temperature. *Nat Commun* 4:Artn 2931. <https://doi.org/10.1038/Ncomms3931>
51. Chin AH, Vaddiraju S, Maslov AV, Ning CZ, Sunkara MK, Meyyappan M (2006) Near-infrared semiconductor subwavelength-wire lasers. *Appl Phys Lett* 88(16):241
52. Gao Q, Saxena D, Wang F, Fu L, Mokkalapati S, Guo YA, Li L, Wong-Leung J, Caroff P, Tan HH, Jagadish C (2014) Selective-area epitaxy of pure Wurtzite InP nanowires: high quantum efficiency and room-temperature lasing. *Nano Lett* 14(9):5206–5211. <https://doi.org/10.1021/nl5021409>
53. Zhang LJ, Luo JW, Zunger A, Akopian N, Zwiller V, Harmand JC (2010) Wide InP nanowires with Wurtzite/Zincblende Superlattice segments are type-II whereas narrower nanowires become type-I: an atomistic pseudopotential calculation. *Nano Lett* 10(10):4055–4060. <https://doi.org/10.1021/nl102109s>
54. Zhang CF, Zhang F, Xia T, Kumar N, Hahm JI, Liu J, Wang ZL, Xu J (2009) Low-threshold two-photon pumped ZnO nanowire lasers. *Opt Express* 17(10):7893–7900
55. Duan XF, Huang Y, Agarwal R, Lieber CM (2003) Single-nanowire electrically driven lasers. *Nature* 421(6920):241–245. <https://doi.org/10.1038/nature01353>
56. Green MA, Ho-Baillie A, Snaith HJ (2014) The emergence of perovskite solar cells. *Nat Photonics* 8(7):506–514. <https://doi.org/10.1038/Nphoton.2014.134>
57. Snaith HJ (2013) Perovskites: the emergence of a new era for low-cost, high-efficiency solar cells. *J Phys Chem Lett* 4(21):3623–3630. <https://doi.org/10.1021/jz4020162>
58. Xing J, Liu XF, Zhang Q, Ha ST, Yuan YW, Shen C, Sum TC, Xiong QH (2015) Vapor phase synthesis of Organometal halide perovskite nanowires for tunable room-temperature Nanolasers. *Nano Lett* 15(7):4571–4577. <https://doi.org/10.1021/acs.nanolett.5b01166>
59. Zhang Q, Su R, Liu XF, Xing J, Sum TC, Xiong QH (2016) High-quality whispering-gallery-mode lasing from cesium lead halide perovskite Nanoplatelets. *Adv Funct Mater* 26(34):6238–6245. <https://doi.org/10.1002/adfm.201601690>
60. Liu XF, Niu L, Wu CY, Cong CX, Wang H, Zeng QS, He HY, Fu QD, Fu W, Yu T, Jin CH, Liu Z, Sum TC (2016) Periodic organic-inorganic halide perovskite microplatelet arrays on silicon substrates for room-temperature lasing. *Adv Sci* 3(11):Artn 1600137. <https://doi.org/10.1002/AdvS.201600137>
61. Zhu HM, Fu YP, Meng F, Wu XX, Gong ZZ, Ding Q, Gustafsson MV, Trinh MT, Jin S, Zhu XY (2015) Lead halide perovskite nanowire lasers with low lasing thresholds and high quality factors. *Nat Mater* 14(6):636–U115. <https://doi.org/10.1038/NMAT4271>
62. Niu GD, Guo XD, Wang LD (2015) Review of recent progress in chemical stability of perovskite solar cells. *J Mater Chem A* 3(17):8970–8980. <https://doi.org/10.1039/c4ta04994b>
63. Conings B, Drijkoningen J, Gauquelin N, Babayigit A, D’Haen J, D’Olieslaeger L, Ethirajan A, Verbeeck J, Manca J, Mosconi E, De Angelis F, Boyen HG (2015) Intrinsic thermal instability of Methylammonium lead Trihalide perovskite. *Adv Energy Mater* 5(15):Artn 1500477. <https://doi.org/10.1002/Aenm.201500477>
64. Lee JW, Kim DH, Kim HS, Seo SW, Cho SM, Park NG (2015) Formamidinium and cesium hybridization for photo- and moisture-stable perovskite solar cell. *Adv Energy Mater* 5(20):Artn 1501310. <https://doi.org/10.1002/Aenm.201501310>

65. Eaton SW, Lai ML, Gibson NA, Wong AB, Dou LT, Ma J, Wang LW, Leone SR, Yang PD (2016) Lasing in robust cesium lead halide perovskite nanowires. *P Natl Acad Sci USA* 113 (8):1993–1998. <https://doi.org/10.1073/pnas.1600789113>
66. Li JB, Meng C, Liu Y, Wu XQ, Lu YZ, Ye Y, Dai L, Tong LM, Liu X, Yang Q (2013) Wavelength tunable CdSe nanowire lasers based on the absorption-emission-absorption process. *Adv Mater* 25(6):833–837. <https://doi.org/10.1002/adma.201203692>
67. Liu XF, Zhang Q, Yip JN, Xiong QH, Sum TC (2013) Wavelength tunable single nanowire lasers based on surface Plasmon Polariton enhanced Burstein-Moss effect. *Nano Lett* 13 (11):5336–5343. <https://doi.org/10.1021/nl402836x>
68. Pauzauskie PJ, Sirbully DJ, Yang PD (2006) Semiconductor nanowire ring resonator laser. *Phys Rev Lett* 96(14):Art143903. <https://doi.org/10.1103/Physrevlett.96.143903>
69. Liu XF, Zhang Q, Xiong QH, Sum TC (2013) Tailoring the lasing modes in semiconductor nanowire cavities using intrinsic self-absorption. *Nano Lett* 13(3):1080–1085. <https://doi.org/10.1021/nl304362u>
70. Liu YK, Zapien JA, Shan YY, Geng CY, Lee CS, Lee ST (2005) Wavelength-controlled lasing in ZnxCd1-xS single-crystal nanoribbons. *Adv Mater* 17(11):1372–1377. <https://doi.org/10.1002/adma.200401606>
71. Kuykendall T, Ulrich P, Aloni S, Yang P (2007) Complete composition tunability of InGaN nanowires using a combinatorial approach. *Nat Mater* 6(12):951–956. <https://doi.org/10.1038/nmat2037>
72. Pan AL, Liu RB, Sun MH, Ning CZ (2010) Spatial composition grading of quaternary ZnCdSSe alloy nanowires with tunable light emission between 350 and 710 nm on a single substrate. *ACS Nano* 4(2):671–680. <https://doi.org/10.1021/nn901699h>
73. Ma YG, Li XY, Yang ZY, Yu HK, Wang P, Tong LM (2010) Pigtailed CdS nanoribbon ring laser. *Appl Phys Lett* 97(15):Art153122. <https://doi.org/10.1063/1.3501969>
74. Yang Q, Jiang XS, Guo X, Chen Y, Tong LM (2009) Hybrid structure laser based on semiconductor nanowires and a silica microfiber knot cavity. *Appl Phys Lett* 94(10):101108. <https://doi.org/10.1063/1.3093821>
75. Wang GZ, Jiang XS, Zhao MX, Ma YG, Fan HB, Yang Q, Tong LM, Xiao M (2012) Microlaser based on a hybrid structure of a semiconductor nanowire and a silica microdisk cavity. *Opt Express* 20(28):29472–29478. <https://doi.org/10.1364/Oe.20.029472>
76. Liu ZC, Yin LJ, Ning H, Yang ZY, Tong LM, Ning CZ (2013) Dynamical color-controllable lasing with extremely wide tuning range from red to green in a single alloy nanowire using nanoscale manipulation. *Nano Lett* 13(10):4945–4950. <https://doi.org/10.1021/nl4029686>
77. Zhang T, Shan F (2014) Development and application of surface plasmon polaritons on optical amplification. *J Nanomater:Art1495381*. <https://doi.org/10.1155/2014/495381>
78. Berini P, De Leon I (2012) Surface plasmon-polariton amplifiers and lasers. *Nat Photonics* 6 (1):16–24. <https://doi.org/10.1038/nphoton.2011.285>
79. Maslov AV, Ning CZ (2007) Size reduction of a semiconductor nanowire laser by using metal coating. *Proc Spie* 6468:Art164680i. <https://doi.org/10.1117/12.723786>
80. Oulton RF, Sorger VJ, Genov DA, Pile DFP, Zhang X (2008) A hybrid plasmonic waveguide for subwavelength confinement and long-range propagation. *Nat Photonics* 2(8):496–500. <https://doi.org/10.1038/nphoton.2008.131>
81. Oulton RF, Sorger VJ, Zentgraf T, Ma RM, Gladden C, Dai L, Bartal G, Zhang X (2009) Plasmon lasers at deep subwavelength scale. *Nature* 461(7264):629–632. <https://doi.org/10.1038/nature08364>
82. Lu YJ, Kim J, Chen HY, Wu CH, Dabidian N, Sanders CE, Wang CY, Lu MY, Li BH, Qiu XG, Chang WH, Chen LJ, Shvets G, Shih CK, Gwo S (2012) Plasmonic Nanolaser using Epitaxially grown silver film. *Science* 337(6093):450–453. <https://doi.org/10.1126/science.1223504>
83. Zhang Q, Li GY, Liu XF, Qian F, Li Y, Sum TC, Lieber CM, Xiong QH (2014) A room temperature low-threshold ultraviolet plasmonic nanolaser. *Nat Commun* 5:Art4953. <https://doi.org/10.1038/Ncomms5953>

84. Zhang Q, Shan XY, Feng X, Wang CX, Wang QQ, Jia JF, Xue QK (2011) Modulating resonance modes and Q value of a CdS nanowire cavity by single ag nanoparticles. *Nano Lett* 11(10):4270–4274. <https://doi.org/10.1021/nl2022674>
85. Khurgin JB (2015) How to deal with the loss in plasmonics and metamaterials. *Nat Nanotechnol* 10(1):2–6. <https://doi.org/10.1038/nnano.2014.310>
86. Hill MT, Oei YS, Smalbrugge B, Zhu Y, De Vries T, Van Veldhoven PJ, Van Otten FWM, Eijkemans TJ, Turkiewicz JP, De Waardt H, Geluk EJ, Kwon SH, Lee YH, Notzel R, Smit MK (2007) Lasing in metallic- coated nanocavities. *Nat Photonics* 1(10):589–594. <https://doi.org/10.1038/nphoton.2007.171>
87. Li KH, Liu X, Wang Q, Zhao S, Mi Z (2015) Ultralow-threshold electrically injected AlGaIn nanowire ultraviolet lasers on Si operating at low temperature. *Nat Nanotechnol* 10(2):140–144. <https://doi.org/10.1038/Nnano.2014.308>